

pubs.acs.org/JPCB Article

# Measuring Excess Heat Capacities of Deoxyribonucleic Acid (DNA) Folding at the Single-Molecule Level

David A. Nicholson, Bin Jia, and David J. Nesbitt\*



Cite This: https://doi.org/10.1021/acs.jpcb.1c05555

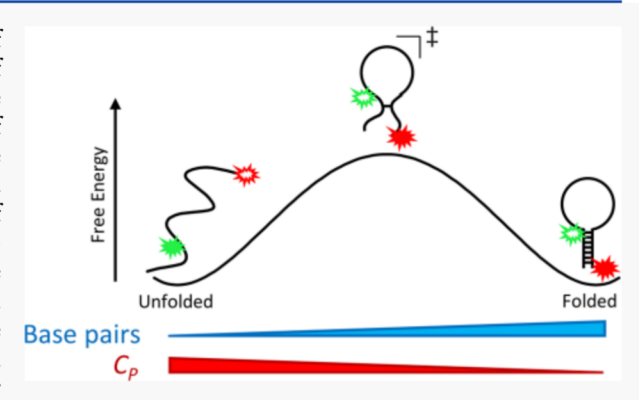


ACCESS I

III Metrics & More

Article Recommendations

**ABSTRACT:** Measurements of the thermodynamic properties of biomolecular folding  $(\Delta G^{\circ}, \Delta H^{\circ}, \Delta S^{\circ}, \text{ etc.})$  provide a wealth of information on the folding process and have long played a central role in biophysical investigation. In particular, the excess heat capacity of folding  $(\Delta C_{\rm P})$  is crucial, as typically measured in bulk ensemble studies by differential scanning calorimetry (DSC) and isothermal titration calorimetry (ITC). Here, we report the first measurements of  $\Delta C_{\rm P}$  at the single-molecule level using the single-molecule fluorescence resonance energy transfer (smFRET) as well as the very first measurements of the heat capacity change associated with achieving the transition state  $(\Delta C^{\ddagger}_{\rm P})$  for nucleic acid folding. The deoxyribonucleic acid (DNA) hairpin used in these studies exhibits an excess heat capacity for hybridization  $(\Delta C_{\rm P} = -340 \pm 60 \,\mathrm{J/mol/K}$  per



base pair) consistent with the range of literature expectations ( $\Delta C_p = -100$  to -420 J/mol/K per base pair). Furthermore, the measured activation heat capacities ( $\Delta C_p^{\ddagger}$ ) for such hairpin unfolding are consistent with a folding transition state containing few fully formed base pairs, in agreement with prevailing models of DNA hybridization.

# 1. INTRODUCTION

The thermodynamics of nucleic acid folding/hybridization is of primary interest to the biophysics community. 1-4 It is widely understood that predicting the temperature stability profile of a deoxyribonucleic acid (DNA) duplex requires knowledge of the folding enthalpy  $\Delta H^{\circ}$  and entropy  $\Delta S^{\circ}$ , as, for instance, often estimated from nearest-neighbor models. 5,6 Less well investigated are heat capacities and, in particular, heat capacity differences between hybridized and unhybridized states, the "excess" heat capacity  $(\Delta C_P)$  for a given conformational transition,  $^{2,7-13}$  which directly affects any predictions for the temperature dependence in  $\Delta H^{\circ}$  and  $\Delta S^{\circ}$ . As a result, the neglect of such excess heat capacity effects results in erroneous extrapolation of nucleic acid folding to conditions other than the reference temperature at which thermodynamic parameters have been determined. Such errors can arise, for example, in the prediction of polymerase chain reaction (PCR) primer stabilities, due to the requisite operation at much higher than body temperatures. As a second example, attempts to unify disparate sets of nearestneighbor model parameters for nucleic acid stabilities have proven challenging due to the need for comparison/ extrapolation between different temperature conditions.<sup>13</sup> Even beyond such technological concerns, a knowledge of excess heat capacities offers first insights into the microscopic dynamics of solvent restructuring during the folding/hybridization event that is inaccessible from the measurements of  $\Delta H^\circ$  and  $\Delta S^\circ$  alone. <sup>2,7,9,10,14</sup>

The existence of such finite excess heat capacities ( $\Delta C_P \neq 0$ ) in nucleic acid folding is well-established, with the majority of  $\Delta C_{\rm P}$  measurements obtained from precision calorimetric methods under bulk ensemble conditions. Specifically, isothermal titration calorimetry (ITC) represents a precision tool for measuring  $\Delta C_{\rm P}$  in systems of medium- to high-affinity bimolecular association, 2,12,15-17 while differential scanning calorimetry (DSC) is able to sensitively report on  $\Delta C_P$  even for weak association processes as well as unimolecular folding dynamics. 17-20 Ultraviolet (UV) absorption optical detection methods offer yet another alternative, whereby hypochromic shifts in DNA absorbance can be used to determine folding equilibrium constants  $(K_{eq})$ , which are subsequently analyzed via temperature-dependent van't Hoff theory in order to extract  $\Delta C_p$ . Each of these approaches offers a powerful and sensitive window into heat capacity differences associated with

Received: June 23, 2021 Revised: August 4, 2021



biomolecular conformational change, though up until now constrained to equilibrium bulk ensemble conditions.

The last two decades have witnessed considerable interest in extending the thermodynamic study of variables such as  $\Delta G^{\circ}$ ,  $\Delta H^{\circ}$ , and  $\Delta S^{\circ}$  based on single-molecule methods, <sup>21–26</sup> which offer a unique opportunity to probe thermodynamic "landscapes" down at the ultimate single-molecule sensitivity limit. Application of such measurement techniques to  $\Delta C_p$ , however, has proven far more challenging and been notably absent in the single-molecule literature. In particular, temperature-dependent single-molecule folding studies are now relatively straightforward<sup>1,27</sup> but to date have focused exclusively on measurements of folding free energies, enthalpies, and entropies rather than excess heat capacities. Indeed, despite an initial report by Williams et al. on establishing the feasibility of determining  $\Delta C_{\rm P}$  via optical tweezers, <sup>28</sup> 20 years have passed without the publication of any articles utilizing singlemolecule methods to extract  $\Delta C_{\rm p}$ .

In this work, we revisit the prospect for the determination of  $\Delta C_{\rm P}$  at the single-molecule level, based on high-precision temperature-dependent studies with the single-molecule fluorescence resonance energy transfer (smFRET).<sup>23,26</sup> We acknowledge at the outset that ITC and DSC measurements under bulk conditions offer greater sensitivity and precision; our goal is simply to establish the smFRET measurement of  $\Delta C_{\rm P}$  as a viable, alternative tool in the single-molecule toolbox. Although this proves more experimentally challenging than conventional van't Hoff temperature measurements of  $\Delta H^{\circ}$ and  $\Delta S^{\circ}$ , we note that such an approach nevertheless does offer unique new insights into oligomer hybridization dynamics. In particular, the smFRET methods described herein provide additional access to folding kinetics unavailable to ITC and DSC approaches, from which we can report first measurements of excess heat capacities involved in accessing the transition state (i.e.,  $\Delta C_P^{\ddagger}$ ) for hybridization in nucleic acid oligomers.

### 2. METHODS

The smFRET construct used in these studies is a DNA hairpin consisting of a 7-base pair stem and a 40-(dA) adenosine loop, which we have previously characterized. <sup>29,30</sup> As depicted schematically in Figure 1, the construct is fluorescently labeled

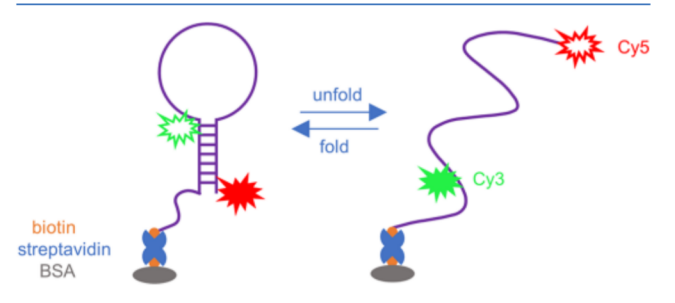


Figure 1. Schematic of DNA hairpin construct used in these studies.

with Cy3 and Cy5 for FRET measurements, and a biotin moiety is attached to the 3' end for surface tethering. The full DNA sequence (5'-Cy5-CTTCAGT- $A_{40}$ -Cy3-ACTGAAG- $A_{11}$ -biotin-3') is purchased in a high-performance liquid chromatography (HPLC) purified form from Integrated DNA Technologies. (Any company names listed herein are in the interest of completeness, not as the endorsement of the vendor.)

Glass surfaces are cleaned and decorated with the smFRET construct in accordance with previously described protocols.  $^{29,31}$  Simply summarized, glass coverslips are soaked in acetone and treated in a UV-ozone cleaner for 30 min. The cleaned coverslips are then exposed, in sequence, to (i) 10%-biotinylated bovine serum albumin (10 mg/mL), (ii) streptavidin (0.2 mg/mL), and finally (iii) the DNA construct (100 pM; 1 pM = 1 pmol/L). The resulting sample has a surface density of ~1 construct per 10  $\mu \rm m^2$ , yielding approximately 100 molecules in the microscopic field of view. Molecules are observed in buffer (50 mM HEPES, pH 7.6) with 120 mM monovalent (K+) ions. To decrease the rate of fluorophore photobleaching, an enzymatic oxygen scavenging cocktail  $^{32}$  (100 nM protocatechuate 3,4-dioxygenase, 5 mM protocatechuic acid, and 2 mM Trolox) is also present.

Single-molecule fluorescence measurements are taken on a through-objective total internal reflection fluorescence (TIRF) microscope. 31,33 Briefly, laser light at 532 nm is focused onto the back focal plane of a high numerical aperture oil-immersion microscope objective, with a pair of mirrors translating the beam off axis to increase the angle of incidence at the sample until total internal reflection is achieved. Widefield fluorescence is collected by the objective and separated by a dichroic mirror into Cy3 and Cy5 emission channels, which are each focused onto a charge-coupled device (CCD) video camera. To increase accuracy when measuring folding rate constants comparable to the CCD frame rate, we exploit stroboscopic excitation methods by modulating the laser to excite the sample for the first 20% of each frame.<sup>34</sup> Single-molecule FRET trajectories are extracted from CCD movies by 31 (i) applying a brightness threshold to locate particles, (ii) summing pixels in a circular neighborhood around each particle to obtain fluorescence rates as a function of time, (iii) subtracting local background, (iv) spatially pairing Cy3 and Cy5 particles by a calibrated affine map,<sup>35</sup> and (v) computing the FRET efficiency, FRET $(t) = I_{\text{CyS}}(t)/(I_{\text{Cy3}}(t) + I_{\text{Cy5}}(t))$ . FRET trajectories are analyzed by dwell time analysis with correction for stroboscopic excitation<sup>34</sup> to yield folding and unfolding rate constants ( $k_{\rm F}$  and  $k_{\rm U}$ ) as well as equilibrium constants  $(K_{eq} = k_F/k_U)$ . Agreement between  $K_{eq}$  values measured by ratios of rate constants to those determined from integrated fractional time spent in the unfolded  $(T_{\rm U})$  vs folded  $(T_{\rm F})$  state  $(K_{\rm eq} = T_{\rm F}/T_{\rm U})$  is routinely at the <2% level.

Sample temperature is controlled using thermoelectric cooling/heating modules under servo loop control, as established previously.<sup>31</sup> To prevent thermal gradients, the sample is heated from above by a module in direct contact with the sample and from below by a module attached to the microscope objective, which maintains thermal contact with the sample by the immersion oil. The system temperature is measured by thermistors, which we have calibrated by in situ measurements of the sample temperature using a thin-wire thermocouple. The thermistor readings are used as an input to the thermoelectric modules for computer-based feedback stabilization with a 0.015 Hz bandwidth, resulting in 0.1 °C temperature accuracy and stability on the 1-min time scale.

# 3. RESULTS

**3.1. Heat Capacity in van't Hoff Analysis.** Measurement of an equilibrium constant at multiple temperatures provides insight into the thermodynamic parameters (enthalpy/entropy) of the underlying process. In particular, the van't

Hoff equation<sup>2</sup> describes the dependence of the equilibrium constant  $K_{eq}$  as a function of overall  $\Delta H^{\circ}$  and entropy  $\Delta S^{\circ}$ :

$$\ln(K_{\rm eq}) = -\frac{\Delta H^{\circ}(T)}{R} \left(\frac{1}{T}\right) + \frac{\Delta S^{\circ}(T)}{R} \tag{1}$$

where T is the absolute temperature and R is the gas constant. Notably, if  $\Delta H^\circ$  and  $\Delta S^\circ$  are independent of temperature, then the resulting van't Hoff plot of  $\ln(K_{\rm eq})$  vs 1/T is predicted to be linear, with slope  $-\Delta H^\circ/R$  and intercept  $\Delta S^\circ/R$ .

If products and reactants have different heat capacities  $C_{\rm p}$ , then the overall reaction will have a nonzero excess heat capacity  $\Delta C_{\rm p} = C_{\rm p}$  (products)  $- C_{\rm p}$  (reactants). The excess heat capacity is related to  $\Delta H^{\circ}$  and  $\Delta S^{\circ}$  by the fundamental thermodynamic expressions<sup>2</sup>

$$\Delta C_{\rm p} = \frac{\partial}{\partial T} (\Delta H^{\circ})_{\rm p} \tag{2}$$

$$\Delta C_{\rm p} = T \frac{\partial}{\partial T} (\Delta S^{\circ})_{\rm p} \tag{3}$$

If  $\Delta C_{\rm P}$  is approximated as a constant over the measured temperature range, we may integrate these equations and substitute the resulting temperature-dependent  $\Delta H^{\circ}(T)$  and  $\Delta S^{\circ}(T)$  into eq 1 to produce the  $\Delta C_{\rm P}$ -modified van't Hoff equation

$$\ln(K_{\rm eq}) = -\frac{\Delta H_{\rm ref}^{\circ}}{R} \left(\frac{1}{T}\right) + \frac{\Delta S_{\rm ref}^{\circ}}{R} - \frac{\Delta C_{\rm p}}{R} \left[ \left(\frac{T - T_{\rm ref}}{T}\right) + \ln\left(\frac{T_{\rm ref}}{T}\right) \right]$$
(4)

where  $T_{\rm ref}$  is an arbitrary reference temperature and  $\Delta H_{\rm ref}^{\circ}$  and  $\Delta S_{\rm ref}^{\circ}$  are  $\Delta H^{\circ}(T)$  and  $\Delta S^{\circ}(T)$  evaluated at  $T_{\rm ref}$  respectively. Most importantly, the additional logarithmic term introduces nonlinearity into the van't Hoff plot, which provides a simple experimental diagnostic for nonzero  $\Delta C_{\rm P}$ .

3.2. smFRET Measurements Reveal Nonzero  $\Delta C_P$  in **DNA Folding.** In order to explore this predicted non-linearity and extract changes in heat capacity, we have measured the folding kinetics of a FRET-labeled DNA hairpin (see Figure 1) as a function of temperature. Across all temperatures (13–35.5 °C), smFRET trajectories exhibit clear switching between two distinct FRET states (see Figure 2), representing unhybridized  $(E_{\rm FRET} \approx 0)$  and hybridized  $(E_{\rm FRET} \approx 0.8)$  conformations. As expected for an exothermic folding process ( $\Delta H^{\circ}$  < 0), the population of the folded state decreases with increasing temperature relative to the unfolded state, corresponding to heat-induced denaturation or "melting" of the DNA hairpin. 3,6 In order to extract the folding/unfolding dynamics in more quantitative detail, we perform dwell time analysis on the smFRET trajectories.<sup>36</sup> At each temperature, the folding and unfolding cumulative dwell time distributions are well-fit by single exponential decays, indicative of simple two-state kinetics governed by the unimolecular rate constants  $k_{\rm F}$  and  $k_{\rm U}$ . From these rate constants, we can directly compute the folding equilibrium constant  $K_{eq} = k_F/k_U$  as a function of

The temperature-dependence of  $K_{\rm eq}$  for the DNA hairpin is presented as a van't Hoff plot in Figure 3. By the way of a first-order treatment, we have analyzed these data with a simple linear fit (Figure 3A, red line), which is equivalent to setting  $\Delta C_{\rm P} = 0$  in Eq. 4. From the fit residuals (Figure 3C), however, the data clearly deviate systematically from such a linear model, with the fit overestimating  $K_{\rm eq}$  at both the lowest and highest

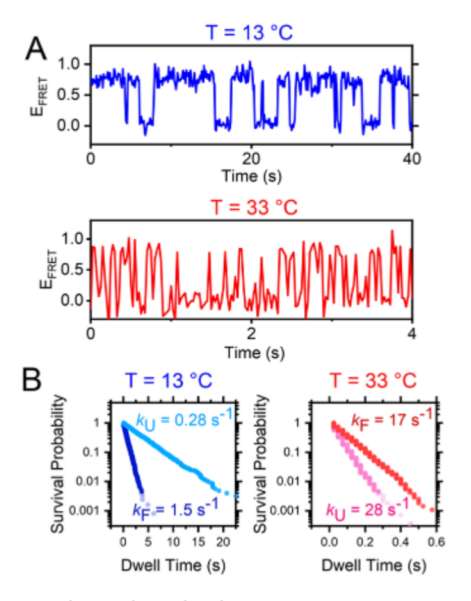


Figure 2. Sample single-molecule FRET time trajectories (A) and dwell time distributions (B) for DNA hairpin folding at 13 and 33 °C.

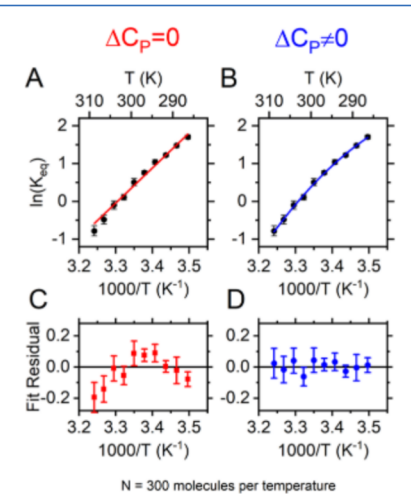


Figure 3. van't Hoff analysis of smFRET-derived equilibrium constants with and without modifications for nonzero excess heat capacity ( $\Delta C_p$ ). (A) Linear van't Hoff fit. (B) Fit with  $\Delta C_p$  term to account for curvature. (C) Fit residuals for the linear fit show systematic deviations away from linearity, while (D) residuals for  $\Delta C_p$ -modified fit exhibit no temperature dependence.

temperatures. To account for such curvature in the van't Hoff plot, we therefore fit the data to the modified van't Hoff equation (eq 4), permitting  $\Delta C_P \neq 0$ . The residuals now exhibit little to no systematic temperature dependence, suggesting a more satisfactory model fit. From a nonlinear weighted least squares fit, we infer the excess heat capacity to be  $\Delta C_P = -2.5 \pm 0.4$  kJ/mol/K, where the uncertainty represents  $1\sigma$  standard deviation. The small fractional uncertainty (<20%) in  $\Delta C_P$  provides additional support for data consistency with nonzero excess heat capacity ( $\Delta C_P \neq 0$ ) upon DNA oligo hybridization.

**3.3.** Arrhenius Analysis of Rate Constants: Transition State Excess Heat Capacity. Temperature-dependent equilibrium constants provide clear evidence for the influence of finite excess heat capacity ( $\Delta C_{\rm P} \neq 0$ ) on the overall DNA hybridization event, as observed herein at the single-molecule level. However, there is also additional thermodynamic

information encoded in the *kinetics* of such single-molecule data, which is not readily accessible in bulk ITC or DSC studies. In particular, we can exploit Arrhenius plots of  $\ln(k)$  vs 1/T to further obtain thermodynamic information about the *transition state* for DNA hybridization. For example, the kinetic data are often fit to the standard Eyring transition state theory (TST) result  $^{37,38}$ 

$$\ln(k) = -\frac{\Delta H^{\ddagger}(T)}{R} \left(\frac{1}{T}\right) + \frac{\Delta S^{\ddagger}(T)}{R} + \ln(\nu^{\ddagger})$$
(5)

where k is the folding or unfolding rate constant,  $\Delta H^{\ddagger}$  is the activation enthalpy,  $\Delta S^{\ddagger}$  is the activation entropy, and  $\nu^{\ddagger}$  is the attempt frequency for the system to reach the transition state. Similar to the van't Hoff analysis (eqs 2–4), we can extend the TST expression in eq 5 to include nonzero excess heat capacity between the transition state and the reactants, yielding

$$\ln(k) = -\frac{\Delta H_{\text{ref}}^{\ddagger}}{R} \left(\frac{1}{T}\right) + \frac{\Delta S_{\text{ref}}^{\ddagger}}{R} - \frac{\Delta C_{\text{p}}^{\ddagger}}{R} \left[ \left(\frac{T - T_{\text{ref}}}{T}\right) + \ln\left(\frac{T_{\text{ref}}}{T}\right) \right] + \ln(\nu^{\ddagger})$$
(6)

where  $\Delta H_{\rm ref}^{\ddagger}$  and  $\Delta S_{\rm ref}^{\ddagger}$  are  $\Delta H^{\ddagger}(T)$  and  $\Delta S^{\ddagger}(T)$  evaluated at the reference temperature  $T_{\rm ref}$ , and  $\Delta C_{\rm P}^{\ddagger}$  is the excess activation heat capacity. Just as in our van't Hoff analysis, a nonzero  $\Delta C_{\rm P}^{\ddagger}$  results in curvature in the Arrhenius plot, which for  $\Delta C_{\rm P}^{\ddagger}=0$  would be perfectly linear. We note that  $\Delta S_{\rm ref}^{\ddagger}$  and  $\ln(\nu^{\ddagger})$  cannot be determined independently of such an analysis, since both parameters are perfectly correlated and simply account for a vertical offset. However, such potential ambiguity in  $\Delta S_{\rm ref}^{\ddagger}$  and  $\ln(\nu^{\ddagger})$  has no effect on  $\Delta C_{\rm P}^{\ddagger}$ , which is a function only of curvature in the temperature-dependent Arrhenius plot. We also note that the applicability of TST to nucleic acid folding is complicated by the presence of multiple folding pathways, as is posited, for instance, in the kinetic zipper model of DNA hybridization (see Section 4). In such a scenario, the measured  $\Delta H_{\rm ref}^{\ddagger}$   $\Delta S_{\rm ref}^{\ddagger}$  and  $\Delta C_{\rm P}^{\ddagger}$  represent a thermal average over these folding pathways.

The temperature-dependent unfolding kinetic measurements for the DNA hairpin are reported in Figure 4A, where the black squares represent experimental data and the solid red and black lines reflect the linear  $(\Delta C_P^{\ddagger} = 0)$  and higher-order,

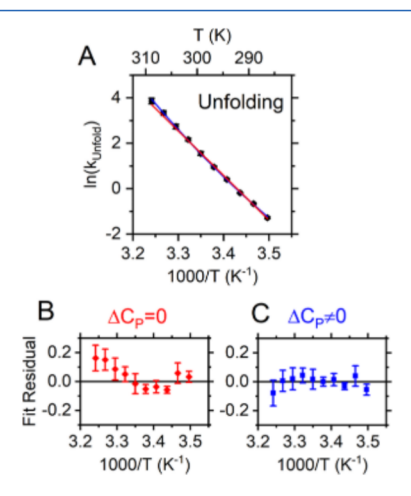
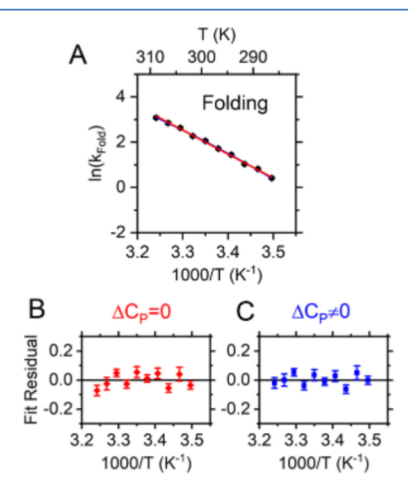


Figure 4. Arrhenius analysis of unfolding rate constant  $k_{\rm U}$ . (A) Data are fit to linear (red) and nonlinear (blue) models. (B) Linear fit residuals exhibit systematic errors compared to (C) nonlinear fit residuals, in support of non-negligible  $\Delta C_{\rm P}$ .

nonlinear approximations  $(\Delta C_p^{\ddagger} \neq 0)$ , respectively. The rate constants increase by more than two orders of magnitude over the temperature range tested, from  $0.28 \pm 0.01 \text{ s}^{-1}$  at 13 °C to  $48 \pm 4 \text{ s}^{-1}$  at 35.5 °C. We have fit these data with both a  $\Delta C_p^{\ddagger}$ = 0 two-parameter fit (eq 5) and a variable  $\Delta C^{\ddagger}_{P} \neq 0$  threeparameter fit (eq 6), with differences between the two fits highlighted by examining the residuals (Figure 4B,C). The residuals for the  $\Delta C_p^{\text{T}} = 0$  fit clearly show systematic temperature-dependent deviations, with the linear fit underestimating measured rate constants at both low and high temperatures. Allowance for a nonzero  $\Delta C^{\ddagger}_{p}$  results in significant improvement, though not as dramatically as for the van't Hoff analysis (Figure 3C,D). To help evaluate the quality of fit (and suitability of the underlying model), we have examined the reduced  $\chi^2$  statistic, which is the average of the square of the residuals divided by their variance  $(\chi^2 = \langle (y_i - y_i) \rangle)$  $y_{i,\text{fit}})^2/\sigma_i^2\rangle$ ), which should be  $\approx 1$  for a physically correct model. For the linear fit  $(\Delta C_P^{\ddagger} = 0)$ , we find  $\chi^2 = 2.7$ , whereas for the nonlinear fit  $(\Delta C_P^{\ddagger} \neq 0)$ ,  $\chi^2 = 0.98$ , which signals clear justification for the higher-level analysis. In summary, the nonlinear least squares fits yield  $\Delta C_{\rm P}^{\ddagger} = 2.3 \pm 0.7 \text{ kJ/mol/K}$  for the excess activation heat capacity between the (i) fully folded and (ii) transition state for unfolding of the smFRET

A similar analysis can of course be performed on  $k_{\rm F}$ , though the curvature in such an Arrhenius plot (see Figure 5) is much



**Figure 5.** Arrhenius analysis of folding rate constant  $k_{\rm F}$ . (A) Linear (red) and nonlinear (blue) fits for  $k_{\rm F}$  are visually indistinguishable. (B) Residuals of the linear fit are unstructured, and (C) introduction of a nonzero  $\Delta C_{\rm F}$  in fitting has little effect on residual errors.

reduced, with a nonzero value of  $\Delta C_P^{\ddagger}$  on the threshold of our experimental resolution. Inspection of the fit residuals shows negligible visible improvement in the residuals upon introducing a nonzero  $\Delta C_P^{\ddagger}$  term. Indeed, this is confirmed by the  $\chi^2$  values for the folding rate constant statistics, which are close to unity for both linear ( $\chi^2=1.7$ ) and nonlinear ( $\chi^2=1.3$ ) fits. Nevertheless, an error-propagated estimate of  $\Delta C_P^{\ddagger}$ ,  $-0.7\pm0.4$  kJ/mol/K, for unfolding kinetic data appears finite, though zero within 95% ( $2\sigma$ ) uncertainty. The results from all fits of the equilibrium and rate constants to van't Hoff and Arrhenius models with finite excess heat capacity are summarized in Table 1.

Table 1. Fit Results of Temperature-Dependent Measurements<sup>a</sup>

	$\Delta H_{\rm ref}^{\circ}$ (kJ/mol)	$\Delta S_{ref}^{\circ}$ (J/mol K)	$\Delta C_{\rm P}$ (kJ/mol K)
	-88 (2)	-294 (8)	-2.5(4)
	$\Delta H_{\rm ref}^{\ddagger}$ (kJ/mol)	$\Delta S_{\text{ref}}^{\ddagger}$ (J/mol K)	$\Delta C_{\rm P}^{\ddagger}$ (kJ/mol K)
folding	85 (2)	57 (7)	-0.7 (4)
unfoldin	g 176 (4)	357 (13)	2.3 (7)

<sup>a</sup>The reference temperature is  $T_{ref} = 300$  K and the attempt frequency is  $\nu^{\ddagger} = 6 \times 10^{12} \text{ s}^{-1}$ . See text for details.

## 4. DISCUSSION

In this work, we have explored the capacity of single-molecule FRET microscopy for measuring excess heat capacities in biomolecular folding. As a proof-of-concept demonstration, we have measured the folding dynamics of a DNA hairpin test system<sup>29,30</sup> (Figure 1) from 13 to 35.5 °C on a single-molecule TIRF microscope. Deviations from the linear behavior in van't Hoff plots of  $K_{eq}$  and Arrhenius plots of  $k_{U}$  (Figures 3 and 4) both indicate clear effects due to nonzero excess heat capacities. From the curvature in these plots, we have extracted differential heat capacities for the overall folding reaction  $(\Delta C_{\rm p})$  and for the approach to the transition state  $(\Delta C_{\rm p}^{\rm T})$  from the reactants and products (Table 1).

The ability to perform such measurements for excess heat capacity  $\Delta C_{\rm P}$  requires the combination of a large temperature range and precise rate-constant measurements. For example, maximal deviations from linearity in the Arrhenius plot for the unfolding rate constant  $k_{\rm U}$  (Figure 4) are only of order  $\approx 0.1$ logarithmic units, which in turn demands <10% fractional uncertainties to observe. We achieve this level of precision by acquiring 20,000 dwell times from 300 molecules for each of 10 different temperatures. Obviously, a high-throughput method such as widefield TIRF microscopy greatly facilitates this level of data acquisition in comparison to confocal microscopy.<sup>25</sup> Such demands on precision can be relaxed if the temperature range is expanded, as the deviations from linearity grow quadratically with  $\Delta T$ . However, the experimentally available range of temperatures is restricted by the stability of the folding, since smFRET kinetic measurements are, in practice, typically limited<sup>36</sup> to systems with  $0.1 \le K_{eq} \le 10$ . It is worth noting that this restriction only applies when measuring equilibrium constants via  $K_{eq} = k_F/k_U$ , with the dynamic range of measurable  $K_{eq}$  values 1-2 orders of magnitude greater if one instead integrates FRET histograms to determine population ratios. The measurement of rate constants is clearly worth the additional effort, however, since such kinetic data provide the additional capacity to measure excess activation heat capacities for accessing the transition state, which represents one unique advantage of using singlemolecule methods over ITC or DSC.

Excess heat capacities in protein and nucleic acid folding are phenomenologically linked to changes in surface area during folding.<sup>2,7,9,10,12,14</sup> The surface area effect has been ascribed to solvent interactions with the nucleic acid, including the hydrophobic effect, perturbations of intramolecular vibrations, and hydrogen bonding.<sup>13</sup> Proteins undergo significant surface area loss during folding, whereas the higher charge densities of polyanionic nucleic acids prevent such compactification. Thus, nucleic acids tend to have smaller specific excess heat capacities than proteins.<sup>13</sup> As a consequence, excess heat capacities in nucleic acids have been more challenging to

measure than for proteins and were indeed once thought to be identically zero. <sup>13</sup> Nonzero  $\Delta C_p$  values for nucleic acid folding are now well-established, <sup>7,43,44</sup> with burial of hydrophobic nucleobases during base pairing considered the primary contributor.

The current single-molecule data for excess heat capacities of nucleic acid folding can be usefully compared with results from bulk calorimetric studies. The specific DNA hairpin construct explored in these studies experiences a decrease in heat capacity upon folding ( $\Delta C_{\rm p} = -2.4 \pm 0.4 \text{ kJ/mol/K}$ ), which is consistent with the general literature consensus of  $\Delta C_{\rm P} < 0$  due to a decrease in accessible surface area. Since the surface area loss is proportional to the number of base pairs formed, and since  $\Delta C_P$  values are at least thought to have only a minor sensitivity to DNA sequence, 12,20 it is convenient to report  $\Delta C_P$  values per base pair, which for our 7 base pair hairpin is  $-340 \pm 60 \text{ J/mol/K/bp}$  (bp = base pair). Previous literature values for  $\Delta C_P$  from bulk studies exhibit a rather broad range from -100 to -420 J/mol/K/bp with a recent metastudy recommending -130 J/mol/K/bp, against which the current single-molecule measurement is high but nevertheless qualitatively consistent. Indeed, the 3-fold dynamic range of these literature results is an indication of the significant experimental challenges involved even in bulk studies of DNA folding as well as additional sensitivity to the nature of the DNA construct.

As a particularly important conformational distinction, most bulk studies have explored duplex formation for bimolecular rather than unimolecular folding, as is the case for the 7 bp DNA hairpin construct connected by a 40-adenine loop utilized in the current single-molecule efforts. Indeed, if we further limit the previous literature comparison only to measurements on unimolecular hairpins, the reported  $\Delta C_{\rm P}$ values grow significantly to -300 J/mol/K/bp, which is now in even better agreement with our single-molecule results. 45-4 Other aspects of single-molecule experimental design can influence duplex stability, including surface tethering 48 and fluorophore incorporation, 49 which may limit comparison with bulk studies of freely diffusing, unlabeled oligonucleotides. Finally, the polyadenosine (poly-dA) loop in the hairpin is known to form single-stranded base-stacked structures<sup>50</sup> which are likely disrupted during folding, leading to an increase in surface area and a concomitant increase in  $C_p$ . Therefore, loop sequences that are less prone to base-stacking, such as polythymidine (poly-dT), may have a more negative  $\Delta C_P$  for folding. These comparisons serve to further highlight the level of complexity in such measurements, with expectations for a possible dependence on loop sequence and GC/AT composition in our smFRET construct.

In addition to the overall heat capacity change during folding  $(\Delta C_{\rm p})$ , we have measured the heat capacity change required to reach the folding transition state  $(\Delta C_P^{\ddagger})$ . While activation heat capacities have been reported for proteins,<sup>51</sup> this work provides, to the best of our knowledge, the first such measurement of  $\Delta C_p^{\ddagger}$  for nucleic acid folding. As one simple check, we confirm that the overall folding heat capacity ( $\Delta C_p$  =  $-2.5 \pm 0.4$  kJ/mol/K) is within uncertainty of the sum of the activation heat capacities  $(\Delta C_{P, \text{ Fold}}^{\ddagger} + (-\Delta C_{P, \text{ Unfold}}^{\ddagger}) = -3.0 \pm$ 0.8 kJ/mol/K), as required since  $C_P$  is a state function. We can combine this information in  $\Delta C_{\rm p}$  and  $\Delta C_{\rm p}^{\ddagger}$  to construct a profile of the system heat capacity "landscape" along the reaction coordinate (Figure 6). If negative excess heat capacities in nucleic acid folding arise primarily from the loss

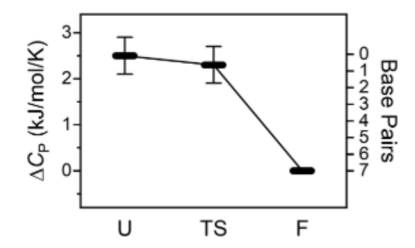


**Figure 6.** Excess heat capacity "landscape" changes along the folding reaction coordinate, relative to the folded state. U = unfolded state, TS = transition state, F = folded state. Note the monotonic decrease in this excess heat capacity upon hybridization of the 7 bp DNA stem and the relatively small activation heat capacity in approaching the transition state from the unfolded direction. The right axis indicates the number of base pairs formed at each state, based on a simple linear model for heat capacity proportional to solvent accessible surface area. Such behavior suggests minimal base pairing at the transition state, which is entirely consistent with "zippering" models for DNA hybridization.<sup>39,40</sup> Error bars reflect one standard error of the mean.

of accessible surface area during base pair formation, as is the literature consensus,  $^{2,13}$  then one consistent expectation is that the heat capacity of the transition state should lie between the folded and unfolded values, since the transition state cannot form more base pairs than the folded state nor less base pairs than the unfolded state. Indeed, the experimental  $\Delta C_{\rm P}$  landscape profile reveals an intermediate transition state heat capacity between that of the unfolded and folded states, in good agreement with this expectation. Interestingly, the transition state excess heat capacity  $C_{\rm P}^{\ddagger}$  appears to be closer to that of the completely unhybridized unfolded state. If one assumes linearity in these excess heat capacities with the hybridization sequence length, this would suggest that relatively few base pairs  $(n_{\rm bp}^{\ddagger}=1\pm1)$  are fully formed in the transition state, certainly including zero within error.

The conclusion that few base pairs are formed at the DNA hairpin's folding transition state is in good agreement with the current kinetic zipper model of nucleic acid hybridization. 39-41,52,53 In the zipper model, the free energy barrier for folding is primarily entropic, as the two DNA strands must "pre-align" in a correct orientation before forming one or more key base pair contact(s).<sup>54</sup> This nucleation site then catalyzes the formation of base pairs at adjacent sites in an enthalpically downhill cascade to the folded state. The number of base pairs in the transition state is a subject of ongoing investigation, with evidence ranging for a transition state containing a single base pair, <sup>55</sup> a minimum of 2 base pairs, <sup>40</sup> or the absence of any nascent base pairs at all. <sup>56,57</sup> Clearly, more work is warranted, and while the uncertainty in our results is too large to resolve these possibilities  $(n_{\text{bp}}^{\ddagger} = 1 \pm 1)$ , our heat capacity-based measurement provides further confirmation of the kinetic zipper prediction of an "early" transition state for hybridization; i.e., a transition state having few if any fully formed base pairs.

### 5. SUMMARY AND CONCLUSION

In this report, we demonstrate the use of smFRET to measure excess and activation heat capacities in biomolecular folding. By combining a large temperature range with high-level data collection statistics, our method achieves the necessary precision to resolve nonzero heat capacities in the folding of a DNA hairpin. The measured value of  $\Delta C_P$  (340  $\pm$  60 J/mol/

K per base pair) is in good agreement with literature calorimetric results on similar constructs, which provides confirming evidence for the accuracy of our method. Furthermore, the present single-molecule studies provide kinetic evidence for finite excess heat capacities upon approach to the transition state  $(\Delta C_P^{\ddagger})$ , which provides novel confirmation that the transition state contains only few fully formed base pairs  $(n_{\rm bp}^{\ddagger}=1\pm1)$  and support of the "kinetic zipper" model for DNA hybridization kinetics. In summary, heat capacity measurements at the single-molecule level offer a useful complement to calorimetric bulk methods and are uniquely capable of inspecting heat capacities of transition states.

#### AUTHOR INFORMATION

## **Corresponding Author**

David J. Nesbitt — JILA, National Institute of Standards and Technology and University of Colorado, Boulder, Colorado 80309, United States; Department of Chemistry and Department of Physics, University of Colorado, Boulder, Colorado 80309, United States; ⊙ orcid.org/0000-0001-5365-1120; Email: djn@jila.colorado.edu

#### **Authors**

David A. Nicholson – JILA, National Institute of Standards and Technology and University of Colorado, Boulder, Colorado 80309, United States; Department of Chemistry, University of Colorado, Boulder, Colorado 80309, United States

Bin Jia – Department of Physics, University of Colorado, Boulder, Colorado 80309, United States

Complete contact information is available at: https://pubs.acs.org/10.1021/acs.jpcb.1c05555

# Notes

The authors declare no competing financial interest.

## ACKNOWLEDGMENTS

Initial support for this work has been through the National Science Foundation under grant CHE-1665271 from the Chemical, Structure, Dynamics, and Mechanisms-A Program, with recent transition support from the Air Force Office of Scientific Research (FA9550-15-1-0090) and additional funds for the development of the TIRF apparatus from PHY-1734006 (Physics Frontier Center Program). We would also like to acknowledge early seed contributions by the W. M. Keck Foundation Initiative in RNA Sciences at the University of Colorado, Boulder. D.A.N. would like to gratefully acknowledge predoctoral fellowship support from the National Institutes of Health Molecular Biophysics Training Grant (T32 GM-065103).

#### REFERENCES

- (1) Holmstrom, E. D.; Nesbitt, D. J. Biophysical insights from temperature-dependent single-molecule Forster resonance energy transfer. *Annu. Rev. Phys. Chem.* **2016**, *67*, 441–465.
- (2) Mikulecky, P. J.; Feig, A. L. Heat capacity changes associated with nucleic acid folding. *Biopolymers* **2006**, *82*, 38–58.
- (3) SantaLucia, J., Jr.; Hicks, D. The thermodynamics of DNA structural motifs. *Annu. Rev. Biophys. Biomol. Struct.* **2004**, 33, 415–440.

- (4) Tsourkas, A.; Behlke, M. A.; Rose, S. D.; Bao, G. Hybridization kinetics and thermodynamics of molecular beacons. *Nucleic Acids Res.* **2003**, *31*, 1319–1330.
- (5) Huguet, J. M.; Bizarro, C. V.; Forns, N.; Smith, S. B.; Bustamante, C.; Ritort, F. Single-molecule derivation of salt dependent base-pair free energies in DNA. *Proc. Natl. Acad. Sci. U. S. A.* **2010**, *107*, 15431–15436.
- (6) SantaLucia, J., Jr. A unified view of polymer, dumbbell, and oligonucleotide DNA nearest-neighbor thermodynamics. *Proc. Natl. Acad. Sci. U. S. A.* **1998**, 95, 1460–1465.
- (7) Dragan, A.; Privalov, P.; Crane-Robinson, C. Thermodynamics of DNA: Heat capacity changes on duplex unfolding. *Eur. Biophys. J.* **2019**, *48*, 773–779.
- (8) Gallagher, K.; Sharp, K. Electrostatic contributions to heat capacity changes of DNA-ligand binding. *Biophys. J.* **1998**, *75*, 769–776.
- (9) Hadzi, S.; Lah, J. Origin of heat capacity increment in DNA folding: The hydration effect. *Biochim. Biophys. Acta, Gen. Subj.* **2021**, 1865, No. 129774.
- (10) Holbrook, J. A.; Capp, M. W.; Saecker, R. M.; Record, M. T., Jr. Enthalpy and heat capacity changes for formation of an oligomeric DNA duplex: Interpretation in terms of coupled processes of formation and association of single-stranded helices. *Biochemistry* 1999, 38, 8409–8422.
- (11) Hughesman, C. B.; Turner, R. F. B.; Haynes, C. Correcting for heat capacity and 5'-TA type terminal nearest neighbors improves prediction of DNA melting temperatures using nearest-neighbor thermodynamic models. *Biochemistry* **2011**, *50*, 2642–2649.
- (12) Mikulecky, P. J.; Feig, A. L. Heat capacity changes associated with DNA duplex formation: Salt- and sequence-dependent effects. *Biochemistry* **2006**, *45*, 604–616.
- (13) Volker, J.; Plum, G. E.; Breslauer, K. J. Heat capacity changes  $(\Delta C_{\rm p})$  for interconversions between differentially-ordered DNA states within physiological temperature domains: Implications for biological regulatory switches. *J. Phys. Chem. B* **2020**, *124*, 5614–5625.
- (14) Cooper, A. Heat capacity effects in protein folding and ligand binding: A re-evaluation of the role of water in biomolecular thermodynamics. *Biophys. Chem.* **2005**, *115*, 89–97.
- (15) Du, X.; Li, Y.; Xia, Y. L.; Ai, S. M.; Liang, J.; Sang, P.; Ji, X. L.; Liu, S. Q. Insights into protein-ligand interactions: Mechanisms, models, and methods. *Int. J. Mol. Sci.* **2016**, *17*, 144.
- (16) Majhi, P. R.; Qi, J.; Tang, C.-F.; Shafer, R. H. Heat capacity changes associated with guanine quadruplex formation: An isothermal titration calorimetry study. *Biopolymers* **2008**, *89*, 302–309.
- (17) Jelesarov, I.; Crane-Robinson, C.; Privalov, P. L. The energetics of HMG box interactions with DNA: Thermodynamic description of the target DNA duplexes. *J. Mol. Biol.* **1999**, *294*, 981–995.
- (18) Jelesarov, I.; Bosshard, H. R. Isothermal titration calorimetry and differential scanning calorimetry as complementary tools to investigate the energetics of biomolecular recognition. *J. Mol. Recognit.* 1999, 12, 3–18.
- (19) Johnson, C. M. Differential scanning calorimetry as a tool for protein folding and stability. *Arch. Biochem. Biophys.* **2013**, 531, 100–109.
- (20) Chalikian, T. V.; Volker, J.; Plum, G. E.; Breslauer, K. J. A more unified picture for the thermodynamics of nucleic acid duplex melting: A characterization by calorimetric and volumetric techniques. *Proc. Natl. Acad. Sci. U. S. A.* **1999**, *96*, 7853–7858.
- (21) Aleman, E. A.; Lamichhane, R.; Rueda, D. Exploring RNA folding one molecule at a time. *Curr. Opin. Chem. Biol.* **2008**, *12*, 647–654.
- (22) Elf, J.; Barkefors, I. Single-molecule kinetics in living cells. *Annu. Rev. Biochem.* **2019**, *88*, 635–659.
- (23) Sustarsic, M.; Kapanidis, A. N. Taking the ruler to the jungle: Single-molecule FRET for understanding biomolecular structure and dynamics in live cells. *Curr. Opin. Struct. Biol.* **2015**, *34*, 52–59.
- (24) Bizzarri, A. R.; Cannistraro, S. The application of atomic force spectroscopy to the study of biological complexes undergoing a biorecognition process. *Chem. Soc. Rev.* **2010**, *39*, 734–749.

- (25) Tan, Y. W.; Hanson, J. A.; Chu, J. W.; Yang, H. Confocal single-molecule FRET for protein conformational dynamics. *Methods Mol. Biol.* **2014**, *1084*, 51–62.
- (26) Lerner, E.; Cordes, T.; Ingargiola, A.; Alhadid, Y.; Chung, S.; Michalet, X.; Weiss, S. Toward dynamic structural biology: Two decades of single-molecule Foerster resonance energy transfer. *Science* **2018**, 359, 288.
- (27) Baker, M. A.; Inoue, Y.; Takeda, K.; Ishijima, A.; Berry, R. M. Two methods of temperature control for single-molecule measurements. *Eur. Biophys. J.* **2011**, *40*, 651–660.
- (28) Williams, M. C.; Wenner, J. R.; Rouzina, I.; Bloomfield, V. A. Entropy and heat capacity of DNA melting from temperature dependence of single molecule stretching. *Biophys. J.* **2001**, *80*, 1932–1939.
- (29) Nicholson, D. A.; Sengupta, A.; Sung, H.-L.; Nesbitt, D. J. Amino acid stabilization of nucleic acid secondary structure: Kinetic insights from single-molecule studies. *J. Phys. Chem. B* **2018**, *122*, 9869–9876.
- (30) Sung, H. L.; Nesbitt, D. J. Single-molecule kinetic studies of DNA hybridization under extreme pressures. *Phys. Chem. Chem. Phys.* **2020**, 22, 23491–23501.
- (31) Nicholson, D. A.; Sengupta, A.; Nesbitt, D. J. Chirality-dependent amino acid modulation of RNA folding. *J. Phys. Chem. B* **2020**, *124*, 11561–11572.
- (32) Aitken, C. E.; Marshall, R. A.; Puglisi, J. D. An oxygen scavenging system for improvement of dye stability in single-molecule fluorescence experiments. *Biophys. J.* **2008**, *94*, 1826–1835.
- (33) Axelrod, D., Total internal reflection fluorescence microscopy. In *Methods in Cell Biology*, 1 ed.; Elsevier Inc.: 2008; Vol. 89, pp. 169–221
- (34) Nicholson, D. A.; Nesbitt, D. J. Pushing camera-based single molecule kinetic measurements to the frame acquisition limit with stroboscopic smFRET. *J. Phys. Chem. B* **2021**, *125*, 6080–6089.
- (35) Cohen, E. A. K.; Ober, R. J., Image registration error analysis with applications in single molecule microscopy. In 2012 9th IEEE International Symposium on Biomedical Imaging (ISBI), 2012; pp. 996–999.
- (36) Kinz-Thompson, C. D.; Bailey, N. A.; Gonzalez, R. L., Precisely and accurately inferring single-molecule rate constants. In *Methods in Enzymology*, Spies, M.; Chemla, Y. R., Eds. Academic Press: 2016; Vol. 581, pp. 187–225.
- (37) Pechukas, P. Transition state theory. *Annu. Rev. Phys. Chem.* **1981**, 32, 159–177.
- (38) Laidler, K. J.; King, M. C. Development of transition-state theory. J. Phys. Chem. 1983, 87, 2657–2664.
- (39) Kuznetsov, S. V.; Ansari, A. A kinetic zipper model with intrachain interactions applied to nucleic acid hairpin folding kinetics. *Biophys. J.* **2012**, *102*, 101–111.
- (40) Ouldridge, T. E.; Sulc, P.; Romano, F.; Doye, J. P.; Louis, A. A. DNA hybridization kinetics: Zippering, internal displacement and sequence dependence. *Nucleic Acids Res.* **2013**, *41*, 8886–8895.
- (41) Yin, Y.; Zhao, X. S. Kinetics and dynamics of DNA hybridization. Acc. Chem. Res. 2011, 44, 1172–1181.
- (42) Taylor, J. R., An introduction to error analysis: The study of uncertainties in physical measurements. University Science Books: 1982.
- (43) Rouzina, I.; Bloomfield, V. A. Heat capacity effects on the melting of DNA. 1. General aspects. *Biophys. J.* **1999**, *77*, 3242–3251.
- (44) Rouzina, I.; Bloomfield, V. A. Heat capacity effects on the melting of DNA. 2. Analysis of nearest-neighbor base pair effects. *Biophys. J.* 1999, 77, 3252–3255.
- (45) Völker, J.; Makube, N.; Plum, G. E.; Klump, H. H.; Breslauer, K. J. Conformational energetics of stable and metastable states formed by DNA triplet repeat oligonucleotides: Implications for triplet expansion diseases. *Proc. Natl. Acad. Sci. U. S. A.* **2002**, *99*, 14700.
- (46) Bourdélat-Parks, B. N.; Wartell, R. M. Thermodynamic stability of DNA tandem mismatches. *Biochemistry* **2004**, *43*, 9918–9925.
- (47) Amrane, S.; Saccà, B.; Mills, M.; Chauhan, M.; Klump, H. H.; Mergny, J.-L. Length-dependent energetics of  $(CTG)_n$  and  $(CAG)_n$  trinucleotide repeats. *Nucleic Acids Res.* **2005**, 33, 4065–4077.

- (48) Roy, R.; Hohng, S.; Ha, T. A practical guide to single-molecule FRET. *Nat. Methods* **2008**, *5*, 507–516.
- (49) Moreira, B. G.; You, Y.; Owczarzy, R. Cy3 and Cy5 dyes attached to oligonucleotide terminus stabilize DNA duplexes: Predictive thermodynamic model. *Biophys. Chem.* **2015**, *198*, 36–44.
- (50) McIntosh, D. B.; Duggan, G.; Gouil, Q.; Saleh, O. A. Sequence-dependent elasticity and electrostatics of single-stranded DNA: Signatures of base-stacking. *Biophys. J.* **2014**, *106*, 659–666.
- (51) Oliveberg, M.; Tan, Y. J.; Fersht, A. R. Negative activation enthalpies in the kinetics of protein folding. *Proc. Natl. Acad. Sci. U. S. A.* 1995, 92, 8926–8929.
- (52) Chen, X.; Zhou, Y.; Qu, P.; Zhao, X. S. Base-by-base dynamics in DNA hybridization probed by fluorescence correlation spectroscopy. *J. Am. Chem. Soc.* **2008**, *130*, 16947–16952.
- (53) He, G.; Li, J.; Ci, H.; Qi, C.; Guo, X. Direct measurement of single-molecule DNA hybridization dynamics with single-base resolution. *Angew. Chem., Int. Ed.* **2016**, *55*, 9036–9040.
- (54) Dupuis, N. F.; Holmstrom, E. D.; Nesbitt, D. J. Single-molecule kinetics reveal cation-promoted DNA duplex formation through ordering of single-stranded helices. *Biophys. J.* **2013**, *105*, 756–766.
- (55) Strunz, T.; Oroszlan, K.; Schafer, R.; Guntherodt, H. J. Dynamic force spectroscopy of single DNA molecules. *Proc. Natl. Acad. Sci. U. S. A.* 1999, 96, 11277–11282.
- (56) Whitley, K. D.; Comstock, M. J.; Chemla, Y. R. Elasticity of the transition state for oligonucleotide hybridization. *Nucleic Acids Res.* **2017**, *45*, 547–555.
- (57) Ho, D.; Zimmermann, J. L.; Dehmelt, F. A.; Steinbach, U.; Erdmann, M.; Severin, P.; Falter, K.; Gaub, H. E. Force-driven separation of short double-stranded DNA. *Biophys. J.* **2009**, *97*, 3158–3167.